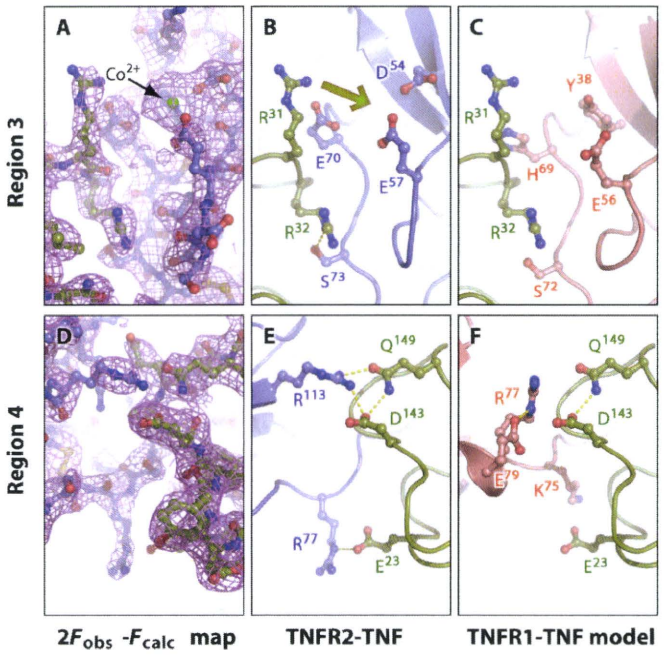

Fig. 4. Difference in the mode of binding of TNF to TNFR1 and TNFR2. Details of the ligand-receptor binding interfaces of TNF-TNFR are shown. (**A** and **D**) $2F_{obs} - F_{calc}$ map of the TNF-TNFR2 complex contoured at 1.0 σ. (**B** and **E**) The TNF-TNFR2 complex. The predicted interaction between R31 of TNF and the acidic surface of TNFR2 (consisting of D54, E57, and E70) is shown as a green arrow. (**C** and **F**) The TNF-TNFR1 model complex. To construct the TNF-TNFR1 model complex, we superimposed the LT-α portion of the LT-α–TNFR1 complex (PDB ID 1tnr) (*23*) onto the TNF portion of the TNF-TNFR2 structure. TNF is in green; TNFR1 is in red; TNFR2 is in blue; the $2F_{obs} - F_{calc}$ map is represented by the pink mesh. Close contacts that are suggestive of potential hydrogen bonds are represented by yellow dashed lines.

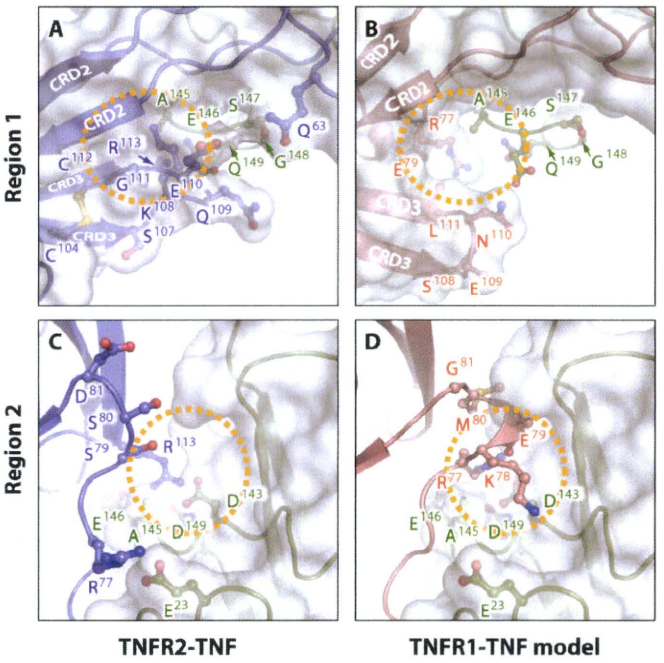

Fig. 5. TNF-TNFR complexes contain a molecular pocket. Difference in the basic structures of TNFR1 and TNFR2. (**A** and **C**) The TNF-TNFR2 complex. (**B** and **D**) The TNF-TNFR1 model complex, which was constructed as described in Fig. 4. TNF is in green; TNFR1 is in red; TNFR2 is in blue. The β strands of CRD2 and CRD3 are indicated by white text. The side chain of Glu[109] is missing in the structure of TNFR1 (PDB ID 1tnr). We observed that a distinct molecular pocket was formed in (B) and (C), which is highlighted by an orange dashed circle.

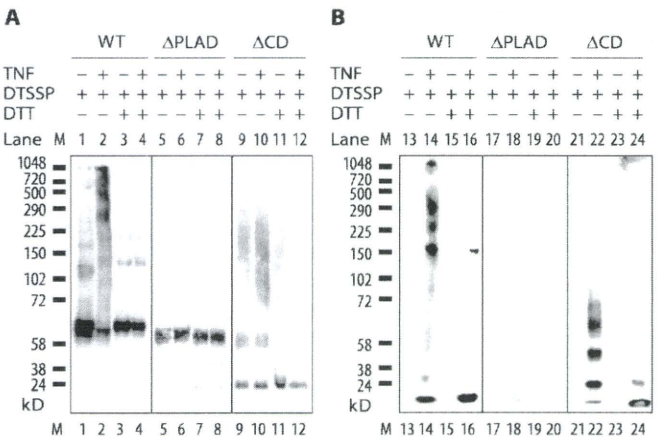

Fig. 6. Formation of TNF-TNFR2 aggregates on the cell surface. (**A** and **B**) TNF-TNFR2 complexes in the plasma membrane of transfected HEK 293T cells were detected by Western blotting analysis with antibodies against (A) the HA epitope and (B) TNF. This result was confirmed by three independent experiments for each group. Predicted molecular masses of related molecules are as follows: HA-wtTNFR2 monomer, 65 kD; HA-wtTNFR2 dimer, 130 kD; HA-wtTNFR2 trimer, 195 kD; TNF monomer, 17 kD; TNF trimer, 51 kD; HA-TNFR2ΔPLAD monomer, 60 kD; HA-TNFR2ΔCD monomer, 25 kD.

We also analyzed the same samples by Western blotting with an antibody against TNF (Fig. 6B). We observed high–molecular mass, TNF-specific bands of >150 kD in samples containing HA-wtTNFR2 and TNF (Fig. 6B, lane 14), but saw only monomeric TNF (17-kD band) under reducing conditions (Fig. 6B, lane 16). This result suggests that TNF molecules were contained in the aggregates of TNFR2 that we observed earlier (Fig. 6A, lane 2). In similar experiments with cells containing HA-TNFR2ΔPLAD, we did not observe TNF-specific bands in any group (Fig. 6B, lanes 17 to 20), indicating that TNF bound rarely to TNFR2ΔPLAD, as was predicted from our earlier results (Fig. 6A). These findings suggest that TNF bound to the PLAD-dependent self-complex of TNFR2 and that the PLAD was a key domain in forming a TNF-TNFR2 aggregate on the cell surface. We could not observe TNF within the self-complex of HA-TNFR2ΔCD (Fig. 6, A and B), indicating that the intracellular domain of TNFR2 also played an important role in forming the TNF-TNFR2 aggregate on the cell surface.

DISCUSSION

Here, we described the first crystal structure of the TNF-TNFR2 complex at a resolution of 3.0 Å. TNF formed a central homotrimer around which were bound three TNFR2 molecules. This overall arrangement was similar

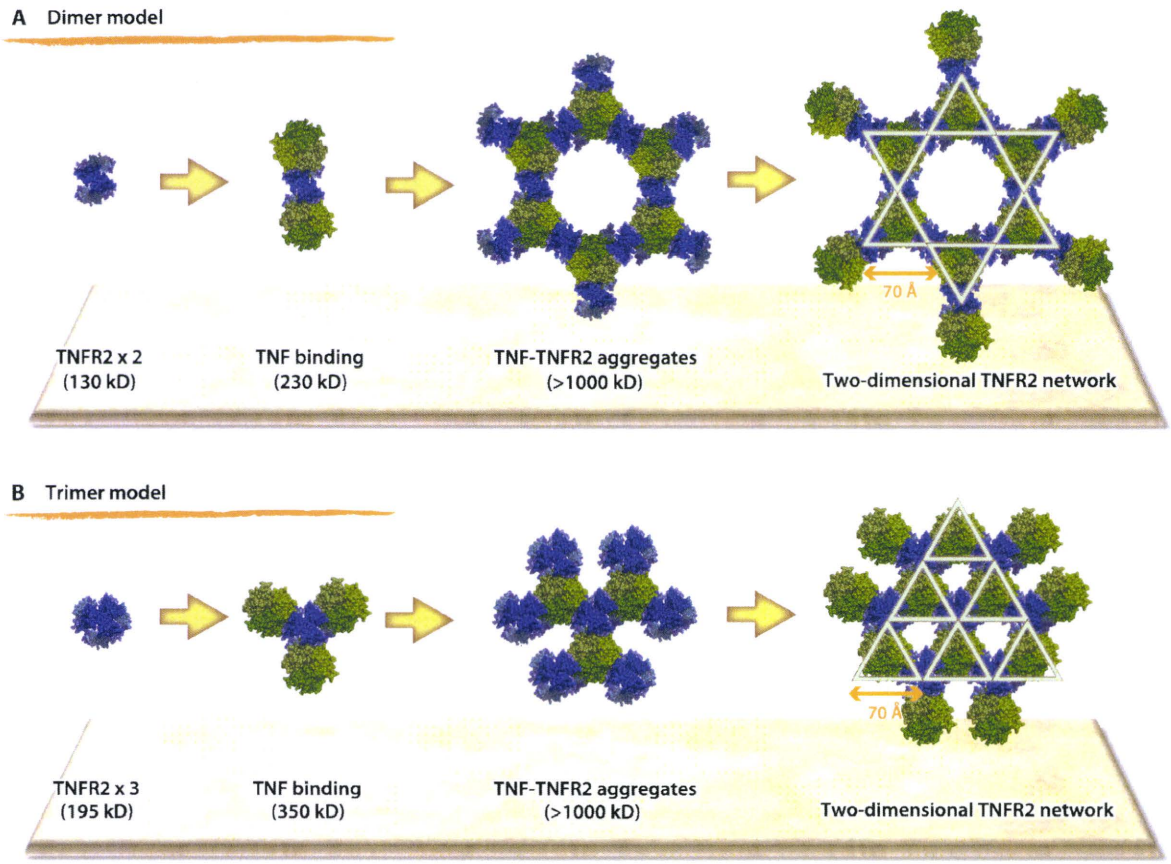

Fig. 7. Structural feasibility of a two-dimensional network model for the initiation of signals through TNFR2. (A and B) Top views of (A) the dimer model and (B) the trimer model of a two-dimensional network of TNFR2. TNFR2 molecules can interact with each other through PLAD-PLAD interactions (deep blue) at the cell surface. TNF trimers can bind around the self-complex of TNFR2. The binding of TNF to TNFR2 may link it to other TNFR2 self-complexes through alternative binding sites, which could result in the formation of a two-dimensional TNF-TNFR2 network. TNF-TNFR2 networks in the dimer and trimer models would maintain six- and threefold symmetry, respectively. These arrangements of TNF-TNFR2 complexes appear to be structurally realistic in both models. The extracellular domain of TNFR2 is in blue and TNF is in green.

to those of other members of the TNF superfamily, including LT-α–TNFR1 (*23*), TRAIL-DR5 (*26–28*), and OX40L-OX40 (*29*) (Fig. 3). However, our determination of the crystal structure of TNFR2 revealed subtle differences with that of TNFR1. The basic structure of TNFR2 differed from that of TNFR1 mainly as a result of variation in the configuration of the folding module. These structural differences altered the mode of ligand recognition of each receptor (Figs. 4 and 5). The results contribute to our understanding of how TNF is able to discriminate between the common binding areas of these two different receptors. In addition, we have already created many mutant TNFs that exhibit different receptor selectivities (*39*, *46*, *50*, *51*). The structures of these mutants and TNF-TNFR complexes are potentially useful to analyze "consensus" information that is essential for the TNF-TNFR interaction (*52*). Such information will be useful in the future for enhancing accuracy in the rational design of new drugs, such as TNFR-selective inhibitors.

We also revealed the formation of an aggregate of TNFR2 on the cell surface (Fig. 6). These aggregates contained both TNF and TNFR2, which indicated that an aggregate of TNF-TNFR2 complexes (>1000 kD) was present on the cell surface. This result was observed in cells transfected to express TNFR2 at the surface and needs to be confirmed by another experimental method in primary cells in the future. However, the importance of such TNF-TNFR2 aggregates in the initiation of TNFR signaling can also be predicted from a previous report on TNF heterotrimers that contained inactive, mutant TNF molecules that acted as dominant-negative TNF because of their lack of trivalent binding potency (*53*).

The HA-TNFR2ΔCD mutant formed a self-complex, but not an aggregate of TNF and TNFR2. Because the structure of the intracellular domain of TNFR2 is still unknown, we are unable to discuss the implications of these findings in detail. Nonetheless, we can speculate that the arrangement of the intracellular domain of TNFR2 might be important for the formation of aggregates of TNF and TNFR2 on the cell surface. Our deletion experiment with HA-TNFR2ΔPLAD indicated that the TNFR2 self-complex forms through PLAD-PLAD interactions, resulting in generation of the TNF-TNFR2 aggregate; however, despite the possibility of the formation of the TNF-TNFR2 complex through PLAD-mediated interactions, we observed that the PLADs of each TNFR2 were dissociated in the crystal structure (Fig. 3). To resolve this apparent contradiction in TNF-mediated signal initiation, we used a structure-based hypothesis based on information concerning our observation of TNF-TNFR2 aggregates of >1000 kD and the crystal structure of TNFR2.

Regarding our prediction of the configuration of the TNFR on the cell surface, previous studies showed that two types of ligand-free TNFR1 proteins form dimers in crystal structures, which are termed parallel dimers at pH 7.5 (*54*) and antiparallel dimers at pH 3.7 (*55*). The TNFR1 parallel dimer forms through PLAD-PLAD interactions in the crystal, and it has been speculated that such a dimer may also be formed on the cell surface (*54*); however, our data (Fig. 6) and another report (*33*) suggest that TNFR1 and TNFR2 form a self-complex as homodimers or homotrimers on the cell surface. Given that the stoichiometry of the TNFR2 self-complex is unclear, these findings imply two possible models for the complex (dimer and trimer models) (Fig. 7). In these models, two or three TNF trimers bind around a central dimer or trimer of TNFR2 molecules, respectively. Other self-complexes of TNFR2 are subsequently recruited to bind around the TNFs, generating an aggregate of TNF-TNFR2 in a two-dimensional network on the cell surface. TNF-TNFR2 networks in the dimer and trimer models would maintain six- and threefold symmetries, respectively. The crystal structure of the TNF-TNFR2 complex suggests that these arrangements of complexes appear to be structurally realistic in both models. This structural feasibility will strengthen a predicted two-dimensional network model described previously (*54*, *56*). Finally, expansion of the network may influence the arrangement of the intracellular domains of TNFR2, thereby possibly inducing the recruitment of intracellular molecules, such as TNFR-associated factor 2 (TRAF2) in TNFR2 signaling.

With respect to TRAF2, we can speculate about its intracellular behavior after the formation of the TNF-TNFR2 aggregate. TRAF2 is essential for TNFR2-mediated signaling. Indeed, the structure of a complex of the C-terminal domain of TRAF2 and a peptide from the intracellular domain of TNFR2 has been reported (*57*). The C-terminal domain of TRAF2 forms a trimer that binds to the intracellular domains of three TNFR2 molecules (*57*); however, there is no structural difference between the peptide-bound form and the unbound form. Therefore, it was unclear how TRAF2 transduces a signal to downstream molecules. The crystal structure of the N-terminal domain of TRAF6, which is homologous to TRAF2, has been solved (*58*). The structure shows that the N-terminal domains of TRAF6 are complexed to each other, suggesting that this interaction forms part of its signaling mechanism. Together, these findings suggest that the TNF-TNFR2 network might organize the intracellular domains of TNFR2 and induce the recruitment of TRAF2, which would result in a TRAF2-TRAF2 intermolecular interaction that is needed for signal transduction. Although this structure-based hypothesis needs to be confirmed by other experiments (for example, role of the intracellular domain and the use of a non–cross-linking methodology such as the direct observation of cell surface complexes with an electron microscope), we suggest that it might provide a new direction for solving the enigma concerning the mechanism of signal initiation of TNFR superfamily members.

The TNF-TNFR2 structures revealed in this report show the diversity in the molecular basis of TNF-TNFR recognition and provide a better understanding of the mechanism of signal initiation by members of the TNFR superfamily. We hope to develop the next generation of therapeutics with an approach based on our structural data, such as new drugs that can selectively inhibit the interaction between one type of TNF-TNFR complex or the formation of one specific type of TNF-TNFR aggregate.

MATERIALS AND METHODS

Data collection and refinement

The complex of amino acid residues 1 to 157 of human TNF (which corresponds to residues 77 to 233 in UniProt P01375) and residues 11 to 183 in human soluble TNFR2 (which corresponds to residues 33 to 205 in UniProt P20333) were prepared as previously described (*38*). The human TNF used in this experiment was mutTNF Lys (−), a lysine-deficient, hexamutant TNF (K11M, K65S, K90P, K98R, K112N, and K128P) with full bioactivity (*40*). This TNF molecule was expressed as inclusion bodies in *Escherichia coli* and refolded as described previously (*38*, *40*). Recombinant human soluble TNFR2 was purchased from PeproTech Inc. (catalog no. 310-12). This TNFR2 molecule was also expressed in *E. coli*. Crystallization and x-ray diffraction experiments were performed as previously described (*38*). Diffraction data were collected at SPring-8 in Harima and Photon Factory in Tsukuba, Japan. The data were indexed, integrated, and scaled with HKL2000 software (*59*). The data set used for structural analysis was collected in BL41XU of SPring-8. Molecular replacement was performed by the MOLREP program (*60*) in CCP4i (*61*) with the structure of the TNF mutant described in our previous report (*39*) (PDB code 2e7a) as a search model. The model from molecular replacement was refined with crystallography and nuclear magnetic resonance (NMR) system (CNS) software (*62*). The Cα chains of TNFR2 molecules were manually traced on the basis of the structure of TNFR1 (PDB code 1tnr) with the Coot program (*63*) in CCP4i. The final structure was refined by the PHENIX program (*64*), and validation of the final model was performed with the RAMPAGE program (*65*) in CCP4i. Data collection statistics (at a resolution of 2.95 Å) were described previously (*38*), and the final structure was refined at a resolution of 3.0 Å. Refinement statistics are given in Table 1. The diffraction data set has a poor R_{merge} value of 0.18, as reported in a previous paper (*38*). This might arise from high and anisotropic mosaicity of the crystals. The gap (6.7%) between the values of R and R_{free} is slightly larger than the 5% that is accepted as no overfitting, which might result from flexible loops with poor electron densities. However, because almost all of the electron densities were interpretable (as shown in Fig. 4, A and D), the overall structure is of sufficient quality to characterize the TNFR2 structure and reveal the recognition mechanism between TNF and TNFR2. All molecular graphics were rendered by PyMOL program (*66*).

Plasmid construction

Plasmids encoding TNFR2 were constructed with the help of a previous report (*33*). Briefly, the leader sequence and the first 10 amino acid residues of full-length, wild-type TNFR2 (wtTNFR2: residues 1 to 32 in UniProt P20333) were connected to the HA epitope tag (YPYDVPDYA) at its C terminus to generate an HA tag fused to the N terminus of TNFR2. Complementary DNAs (cDNAs) of HA-wtTNFR2 (encoding residues 1 to 32–HA–residues 33 to 461 in UniProt P20333), HA-TNFR2ΔPLAD (encoding residues 1 to 32–HA–residues 77 to 461 in UniProt P20333), and HA-TNFR2ΔCD (encoding residues 1 to 32–HA–residues 33 to 287 in UniProt P20333) were amplified and directly cloned into pcDN3.1D/V5-His-TOPO vectors (Invitrogen Corp.). Primers 1 (5′-CACCATGGCGCCCGTCGCCGTCTGGGCCGCGCTGGCCGTCGGACTGGAGCTCTGGGCTGCGGCGCACGCCTTGCCCGCCCAGGTGGCATTTACACCCTACTACCCCTATGATGTGCCAGACTACGCCGCCCCGGAGCCCGGGAGCACATGC-3′) and 3 (5′-TTAACTGGGCTTCATCCCAGCATC-3′) were used to amplify HA-wtTNFR2, whereas primers 2 (5′-CACCATGGCGCCCGTCGCCGTCTGGGCCGCGCTGGCCGTCGGACTGGAGCTCTGGGCTGCGGCGCACGCCTTGCCCGCCCAGGTGGCATTTACACCCTACGCCCTACCCCTATGAGGTGCCAGACTATCCTGTGAGGACAGCACATACACC-3′) and 3 were used to amplify HA-TNFR2ΔPLAD cDNA. Primers 1 and 4 (5′-TCACACCTGGGTCATGATGACACAGTT-3′) were used for the amplification of HA-TNFR2ΔCD.

Expression and cross-linking of TNFR2 at the cell surface

HEK 293T cells were cultured in Dulbecco's modified Eagle's medium (DMEM) (Wako Pure Chemical Industries Ltd.), containing 10% fetal

bovine serum at 37°C under 5% CO_2. Cells were transfected with plasmids encoding HA-wtTNFR2, HA-TNFR2ΔPLAD, or HA-TNFR2ΔCD with Lipofectamine LTX and Plus reagent (Invitrogen). After incubation for 6 hours at 37°C under 5% CO_2, TNFR2 proteins were expressed on the surface of the HEK 293T cells. For cells treated with TNF, recombinant human TNF (R&D Systems Inc.) was added to the cells at a final concentration of 5 μg/ml, and the cells were then incubated at 4°C for 1 hour. Cells were scraped from the culture dish and incubated in 1 mM DTSSP (Thermo Fisher Scientific Inc.) for 30 min at room temperature to cross-link cell surface TNFR2 complexes. The cross-linking reaction was terminated by the addition of 20 mM tris-HCl (pH 7.4). Membrane proteins, which contained cell surface TNFR2 complexes, were purified with the Plasma Membrane Protein Extraction Kit (BioVision).

Western blotting analysis

Purified membrane proteins were mixed with an equal volume of Laemmli sample buffer (Bio-Rad Laboratories Inc.) with or without 50 mM DTT (Thermo Fisher Scientific). The samples were subjected to SDS–polyacrylamide gel electrophoresis (SDS-PAGE) with a 3 to 10% gradient polyacrylamide gel (ATTO Corp.). Proteins were then transferred onto a polyvinylidene difluoride (PVDF) membrane (GE Healthcare Bio-Sciences Corp.). We used antibody against the HA epitope (Abcam Inc.) and horseradish peroxidase (HRP)–conjugated antibody against mouse immunoglobulin G (IgG) (GE Healthcare Bio-Sciences) to detect HA-wtTNFR2, HA-TNFR2ΔPLAD, and HA-TNFR2ΔCD proteins. To detect TNF, we used antibody against human TNF (Genzyme Corp.) and HRP-conjugated antibody against mouse IgG. Specific bands were visualized with the ECL Plus reagent (GE Healthcare Bio-Sciences). To estimate the molecular mass of large complexes, we used high–molecular weight markers (NativeMark and HiMark HMW standard; Invitrogen).

REFERENCES AND NOTES

1. B. B. Aggarwal, Signalling pathways of the TNF superfamily: A double-edged sword. *Nat. Rev. Immunol.* **3**, 745–756 (2003).
2. W. M. Kooloos, D. J. de Jong, T. W. Huizinga, H. J. Guchelaar, Potential role of pharmacogenetics in anti-TNF treatment of rheumatoid arthritis and Crohn's disease. *Drug Discov. Today* **12**, 125–131 (2007).
3. P. Rutgeerts, G. Van Assche, S. Vermeire, Optimizing anti-TNF treatment in inflammatory bowel disease. *Gastroenterology* **126**, 1593–1610 (2004).
4. M. Feldmann, R. N. Maini, Lasker Clinical Medical Research Award. TNF defined as a therapeutic target for rheumatoid arthritis and other autoimmune diseases. *Nat. Med.* **9**, 1245–1250 (2003).
5. M. G. Tansey, D. E. Szymkowski, The TNF superfamily in 2009: New pathways, new indications, and new drugs. *Drug Discov. Today* **14**, 1082–1088 (2009).
6. R. O. Williams, M. Feldmann, R. N. Maini, Anti-tumor necrosis factor ameliorates joint disease in murine collagen-induced arthritis. *Proc. Natl. Acad. Sci. U.S.A.* **89**, 9784–9788 (1992).
7. G. J. Thorbecke, R. Shah, C. H. Leu, A. P. Kuruvilla, A. M. Hardison, M. A. Palladino, Involvement of endogenous tumor necrosis factor α and transforming growth factor β during induction of collagen type II arthritis in mice. *Proc. Natl. Acad. Sci. U.S.A.* **89**, 7375–7379 (1992).
8. J. S. Lubel, A. G. Testro, P. W. Angus, Hepatitis B virus reactivation following immunosuppressive therapy: Guidelines for prevention and management. *Intern. Med. J.* **37**, 705–712 (2007).
9. J. J. Gomez-Reino, L. Carmona, V. R. Valverde, E. M. Mola, M. D. Montero, BIOBADASER Group, Treatment of rheumatoid arthritis with tumor necrosis factor inhibitors may predispose to significant increase in tuberculosis risk: A multicenter active-surveillance report. *Arthritis Rheum.* **48**, 2122–2127 (2003).
10. S. L. Brown, M. H. Greene, S. K. Gershon, E. T. Edwards, M. M. Braun, Tumor necrosis factor antagonist therapy and lymphoma development: Twenty-six cases reported to the Food and Drug Administration. *Arthritis Rheum.* **46**, 3151–3158 (2002).
11. D. Faustman, M. Davis, TNF receptor 2 pathway: Drug target for autoimmune diseases. *Nat. Rev. Drug Discov.* **9**, 482–493 (2010).
12. L. Mori, S. Iselin, G. De Libero, W. Lesslauer, Attenuation of collagen-induced arthritis in 55-kDa TNF receptor type 1 (TNFR1)-IgG1-treated and TNFR1-deficient mice. *J. Immunol.* **157**, 3178–3182 (1996).
13. M. Leist, F. Gantner, S. Jilg, A. Wendel, Activation of the 55 kDa TNF receptor is necessary and sufficient for TNF-induced liver failure, hepatocyte apoptosis, and nitrite release. *J. Immunol.* **154**, 1307–1316 (1995).
14. E. Y. Kim, J. J. Priatel, S. J. Teh, H. S. Teh, TNF receptor type 2 (p75) functions as a costimulator for antigen-driven T cell responses in vivo. *J. Immunol.* **176**, 1026–1035 (2006).
15. E. Y. Kim, H. S. Teh, TNF type 2 receptor (p75) lowers the threshold of T cell activation. *J. Immunol.* **167**, 6812–6820 (2001).
16. M. Grell, F. M. Becke, H. Wajant, D. N. Mannel, P. Scheurich, TNF receptor type 2 mediates thymocyte proliferation independently of TNF receptor type 1. *Eur. J. Immunol.* **28**, 257–263 (1998).
17. M. Grell, E. Douni, H. Wajant, M. Lohden, M. Clauss, B. Maxeiner, S. Georgopoulos, W. Lesslauer, G. Kollias, K. Pfizenmaier, P. Scheurich, The transmembrane form of tumor necrosis factor is the prime activating ligand of the 80 kDa tumor necrosis factor receptor. *Cell* **83**, 793–802 (1995).
18. B. M. Saunders, S. Tran, S. Ruuls, J. D. Sedgwick, H. Briscoe, W. J. Britton, Transmembrane TNF is sufficient to initiate cell migration and granuloma formation and provide acute, but not long-term, control of *Mycobacterium tuberculosis* infection. *J. Immunol.* **174**, 4852–4859 (2005).
19. M. L. Olleros, R. Guler, N. Corazza, D. Vesin, H. P. Eugster, G. Marchal, P. Chavarot, C. Mueller, I. Garcia, Transmembrane TNF induces an efficient cell-mediated immunity and resistance to *Mycobacterium bovis* bacillus Calmette-Guerin infection in the absence of secreted TNF and lymphotoxin-α. *J. Immunol.* **168**, 3394–3401 (2002).
20. X. Chen, M. Baumel, D. N. Mannel, O. M. Howard, J. J. Oppenheim, Interaction of TNF with TNF receptor type 2 promotes expansion and function of mouse $CD4^+CD25^+$ T regulatory cells. *J. Immunol.* **179**, 154–161 (2007).
21. R. E. Kontermann, P. Scheurich, K. Pfizenmaier, Antagonists of TNF action: Clinical experience and new developments. *Expert Opin. Drug Discov.* **4**, 279–292 (2009).
22. G. Kollias, D. Kontoyiannis, Role of TNF/TNFR in autoimmunity: Specific TNF receptor blockade may be advantageous to anti-TNF treatments. *Cytokine Growth Factor Rev.* **13**, 315–321 (2002).
23. D. W. Banner, A. D'Arcy, W. Janes, R. Gentz, H. J. Schoenfeld, C. Broger, H. Loetscher, W. Lesslauer, Crystal structure of the soluble human 55 kd TNF receptor-human TNFβ complex: Implications for TNF receptor activation. *Cell* **73**, 431–445 (1993).
24. E. Y. Jones, D. I. Stuart, N. P. Walker, Structure of tumour necrosis factor. *Nature* **338**, 225–228 (1989).
25. M. J. Eck, S. R. Sprang, The structure of tumor necrosis factor-α at 2.6 Å resolution. Implications for receptor binding. *J. Biol. Chem.* **264**, 17595–17605 (1989).
26. S. S. Cha, B. J. Sung, Y. A. Kim, Y. L. Song, H. J. Kim, S. Kim, M. S. Lee, B. H. Oh, Crystal structure of TRAIL-DR5 complex identifies a critical role of the unique frame insertion in conferring recognition specificity. *J. Biol. Chem.* **275**, 31171–31177 (2000).
27. J. Mongkolsapaya, J. M. Grimes, N. Chen, X. N. Xu, D. I. Stuart, E. Y. Jones, G. R. Screaton, Structure of the TRAIL-DR5 complex reveals mechanisms conferring specificity in apoptotic initiation. *Nat. Struct. Biol.* **6**, 1048–1053 (1999).
28. S. G. Hymowitz, H. W. Christinger, G. Fuh, M. Ultsch, M. O'Connell, R. F. Kelley, A. Ashkenazi, A. M. de Vos, Triggering cell death: The crystal structure of Apo2L/TRAIL in a complex with death receptor 5. *Mol. Cell* **4**, 563–571 (1999).
29. D. M. Compaan, S. G. Hymowitz, The crystal structure of the costimulatory OX40-OX40L complex. *Structure* **14**, 1321–1330 (2006).
30. Z. Yang, A. P. West Jr., P. J. Bjorkman, Crystal structure of TNFα complexed with a poxvirus MHC-related TNF binding protein. *Nat. Struct. Mol. Biol.* **16**, 1189–1191 (2009).
31. M. M. Rahman, A. R. Lucas, G. McFadden, Viral TNF inhibitors as potential therapeutics. *Adv. Exp. Med. Biol.* **666**, 64–77 (2009).
32. R. M. Siegel, J. K. Frederiksen, D. A. Zacharias, F. K. Chan, M. Johnson, D. Lynch, R. Y. Tsien, M. J. Lenardo, Fas preassociation required for apoptosis signaling and dominant inhibition by pathogenic mutations. *Science* **288**, 2354–2357 (2000).
33. F. K. Chan, H. J. Chun, L. Zheng, R. M. Siegel, K. L. Bui, M. J. Lenardo, A domain in TNF receptors that mediates ligand-independent receptor assembly and signaling. *Science* **288**, 2351–2354 (2000).
34. L. M. Sedger, S. R. Osvath, X. M. Xu, G. Li, F. K. Chan, J. W. Barrett, G. McFadden, Poxvirus tumor necrosis factor receptor (TNFR)-like T2 proteins contain a conserved preligand assembly domain that inhibits cellular TNFR1-induced cell death. *J. Virol.* **80**, 9300–9309 (2006).
35. L. Clancy, K. Mruk, K. Archer, M. Woelfel, J. Mongkolsapaya, G. Screaton, M. J. Lenardo, F. K. Chan, Preligand assembly domain-mediated ligand-independent association between TRAIL receptor 4 (TR4) and TR2 regulates TRAIL-induced apoptosis. *Proc. Natl. Acad. Sci. U.S.A.* **102**, 18099–18104 (2005).
36. J. M. Kramer, W. Hanel, F. Shen, N. Isik, J. P. Malone, A. Maitra, W. Sigurdson, D. Swart, J. Tocker, T. Jin, S. L. Gaffen, Cutting edge: Identification of a pre-ligand assembly domain (PLAD) and ligand binding site in the IL-17 receptor. *J. Immunol.* **179**, 6379–6383 (2007).
37. G. M. Deng, L. Zheng, F. K. Chan, M. Lenardo, Amelioration of inflammatory arthritis by targeting the pre-ligand assembly domain of tumor necrosis factor receptors. *Nat. Med.* **11**, 1066–1072 (2005).

38. Y. Mukai, T. Nakamura, Y. Yoshioka, S. Tsunoda, H. Kamada, S. Nakagawa, Y. Yamagata, Y. Tsutsumi, Crystallization and preliminary x-ray analysis of the tumour necrosis factor α-tumour necrosis factor receptor type 2 complex. *Acta Crystallogr. Sect. F Struct. Biol. Cryst. Commun.* **65**, 295–298 (2009).
39. H. Shibata, Y. Yoshioka, A. Ohkawa, K. Minowa, Y. Mukai, Y. Abe, M. Taniai, T. Nomura, H. Kayamuro, H. Nabeshi, T. Sugita, S. Imai, K. Nagano, T. Yoshikawa, T. Fujita, S. Nakagawa, A. Yamamoto, T. Ohta, T. Hayakawa, T. Mayumi, P. Vandenabeele, B. B. Aggarwal, T. Nakamura, Y. Yamagata, S. Tsunoda, H. Kamada, Y. Tsutsumi, Creation and x-ray structure analysis of the tumor necrosis factor receptor-1-selective mutant of a tumor necrosis factor-α antagonist. *J. Biol. Chem.* **283**, 998–1007 (2008).
40. Y. Yamamoto, Y. Tsutsumi, Y. Yoshioka, T. Nishibata, K. Kobayashi, T. Okamoto, Y. Mukai, T. Shimizu, S. Nakagawa, S. Nagata, T. Mayumi, Site-specific PEGylation of a lysine-deficient TNF-α with full bioactivity. *Nat. Biotechnol.* **21**, 546–552 (2003).
41. E. Oregon-Romero, M. Vazquez-Del Mercado, R. E. Navarro-Hernandez, N. Torres-Carrillo, G. Martinez-Bonilla, I. Estrada-Garcia, H. Rangel-Villalobos, J. F. Munoz-Valle, Tumor necrosis factor receptor 2 M196R polymorphism in rheumatoid arthritis and osteoarthritis: Relationship with sTNFR2 levels and clinical features. *Rheumatol. Int.* **27**, 53–59 (2006).
42. C. Morita, T. Horiuchi, H. Tsukamoto, N. Hatta, Y. Kikuchi, Y. Arinobu, T. Otsuka, T. Sawabe, S. Harashima, K. Nagasawa, Y. Niho, Association of tumor necrosis factor receptor type II polymorphism 196R with systemic lupus erythematosus in the Japanese: Molecular and functional analysis. *Arthritis Rheum.* **44**, 2819–2827 (2001).
43. N. Tsuchiya, T. Komata, M. Matsushita, J. Ohashi, K. Tokunaga, New single nucleotide polymorphisms in the coding region of human TNFR2: Association with systemic lupus erythematosus. *Genes Immun.* **1**, 501–503 (2000).
44. J. H. Naismith, S. R. Sprang, Modularity in the TNF-receptor family. *Trends Biochem. Sci.* **23**, 74–79 (1998).
45. S. C. Graham, M. W. Bahar, N. G. Abrescia, G. L. Smith, D. I. Stuart, J. M. Grimes, Structure of CrmE, a virus-encoded tumour necrosis factor receptor. *J. Mol. Biol.* **372**, 660–671 (2007).
46. Y. Mukai, H. Shibata, T. Nakamura, Y. Yoshioka, Y. Abe, T. Nomura, M. Taniai, T. Ohta, S. Ikemizu, S. Nakagawa, S. Tsunoda, H. Kamada, Y. Yamagata, Y. Tsutsumi, Structure–function relationship of tumor necrosis factor (TNF) and its receptor interaction based on 3D structural analysis of a fully active TNFR1-selective TNF mutant. *J. Mol. Biol.* **385**, 1221–1229 (2009).
47. C. Reed, Z. Q. Fu, J. Wu, Y. N. Xue, R. W. Harrison, M. J. Chen, I. T. Weber, Crystal structure of TNF-α mutant R31D with greater affinity for receptor R1 compared with R2. *Protein Eng.* **10**, 1101–1107 (1997).
48. X. Van Ostade, J. Tavernier, W. Fiers, Structure-activity studies of human tumour necrosis factors. *Protein Eng.* **7**, 5–22 (1994).
49. H. Loetscher, D. Stueber, D. Banner, F. Mackay, W. Lesslauer, Human tumor necrosis factor α (TNF α) mutants with exclusive specificity for the 55-kDa or 75-kDa TNF receptors. *J. Biol. Chem.* **268**, 26350–26357 (1993).
50. Y. Mukai, T. Nakamura, Y. Yoshioka, H. Shibata, Y. Abe, T. Nomura, M. Taniai, T. Ohta, S. Nakagawa, S. Tsunoda, H. Kamada, Y. Yamagata, Y. Tsutsumi, Fast binding kinetics and conserved 3D structure underlie the antagonistic activity of mutant TNF: Useful information for designing artificial proteo-antagonists. *J. Biochem.* **146**, 167–172 (2009).
51. H. Shibata, Y. Yoshioka, A. Ohkawa, Y. Abe, T. Nomura, Y. Mukai, S. Nakagawa, M. Taniai, T. Ohta, T. Mayumi, H. Kamada, S. Tsunoda, Y. Tsutsumi, The therapeutic effect of TNFR1-selective antagonistic mutant TNF-α in murine hepatitis models. *Cytokine* **44**, 229–233 (2008).
52. W. L. DeLano, M. H. Ultsch, A. M. de Vos, J. A. Wells, Convergent solutions to binding at a protein-protein interface. *Science* **287**, 1279–1283 (2000).
53. P. M. Steed, M. G. Tansey, J. Zalevsky, E. A. Zhukovsky, J. R. Desjarlais, D. E. Szymkowski, C. Abbott, D. Carmichael, C. Chan, L. Cherry, P. Cheung, A. J. Chirino, H. H. Chung, S. K. Doberstein, A. Eivazi, A. V. Filikov, S. X. Gao, R. S. Hubert, M. Hwang, L. Hyun, S. Kashi, A. Kim, E. Kim, J. Kung, S. P. Martinez, U. S. Muchhal, D. H. Nguyen, C. O'Brien, D. O'Keefe, K. Singer, O. Vafa, J. Vielmetter, S. C. Yoder, B. I. Dahiyat, Inactivation of TNF signaling by rationally designed dominant-negative TNF variants. *Science* **301**, 1895–1898 (2003).
54. J. H. Naismith, T. Q. Devine, B. J. Brandhuber, S. R. Sprang, Crystallographic evidence for dimerization of unliganded tumor necrosis factor receptor. *J. Biol. Chem.* **270**, 13303–13307 (1995).
55. J. H. Naismith, T. Q. Devine, T. Kohno, S. R. Sprang, Structures of the extracellular domain of the type I tumor necrosis factor receptor. *Structure* **4**, 1251–1262 (1996).
56. F. K. Chan, Three is better than one: Pre-ligand receptor assembly in the regulation of TNF receptor signaling. *Cytokine* **37**, 101–107 (2007).
57. Y. C. Park, V. Burkitt, A. R. Villa, L. Tong, H. Wu, Structural basis for self-association and receptor recognition of human TRAF2. *Nature* **398**, 533–538 (1999).
58. Q. Yin, S. C. Lin, B. Lamothe, M. Lu, Y. C. Lo, G. Hura, L. Zheng, R. L. Rich, A. D. Campos, D. G. Myszka, M. J. Lenardo, B. G. Darnay, H. Wu, E2 interaction and dimerization in the crystal structure of TRAF6. *Nat. Struct. Mol. Biol.* **16**, 658–666 (2009).
59. Z. Otwinowski, W. Minor, Processing of x-ray diffraction data collected in oscillation mode. *Methods Enzymol.* **276**, 307–326 (1997).
60. A. Vagin, A. Teplyakov, MOLREP: An automated program for molecular replacement. *J. Appl. Crystallogr.* **30**, 1022–1025 (1997).
61. E. Potterton, P. Briggs, M. Turkenburg, E. Dodson, A graphical user interface to the CCP4 program suite. *Acta Crystallogr. D Biol. Crystallogr.* **59**, 1131–1137 (2003).
62. A. T. Brünger, P. D. Adams, G. M. Clore, W. L. DeLano, P. Gros, R. W. Grosse-Kunstleve, J. S. Jiang, J. Kuszewski, M. Nilges, N. S. Pannu, R. J. Read, L. M. Rice, T. Simonson, G. L. Warren, Crystallography & NMR system: A new software suite for macromolecular structure determination. *Acta Crystallogr. D Biol. Crystallogr.* **54**, 905–921 (1998).
63. P. Emsley, K. Cowtan, Coot: Model-building tools for molecular graphics. *Acta Crystallogr. D Biol. Crystallogr.* **60**, 2126–2132 (2004).
64. P. D. Adams, R. W. Grosse-Kunstleve, L. W. Hung, T. R. Ioerger, A. J. McCoy, N. W. Moriarty, R. J. Read, J. C. Sacchettini, N. K. Sauter, T. C. Terwilliger, PHENIX: Building new software for automated crystallographic structure determination. *Acta Crystallogr. D Biol. Crystallogr.* **58**, 1948–1954 (2002).
65. S. C. Lovell, I. W. Davis, W. B. Arendall III, P. I. de Bakker, J. M. Word, M. G. Prisant, J. S. Richardson, D. C. Richardson, Structure validation by Cα geometry: φ,ψ and Cβ deviation. *Proteins* **50**, 437–450 (2003).
66. W. L. DeLano, *The PyMOL Molecular Graphics System* (DeLano Scientific, San Carlos, CA, 2002), http://www.pymol.org.
67. E. Krissinel, K. Henrick, Secondary-structure matching (SSM), a new tool for fast protein structure alignment in three dimensions. *Acta Crystallogr. D Biol. Crystallogr.* **60**, 2256–2268 (2004).
68. J. D. Thompson, D. G. Higgins, T. J. Gibson, CLUSTAL W: Improving the sensitivity of progressive multiple sequence alignment through sequence weighting, position-specific gap penalties and weight matrix choice. *Nucleic Acids Res.* **22**, 4673–4680 (1994).
69. A. Nicholls, K. A. Sharp, B. Honig, Protein folding and association: Insights from the interfacial and thermodynamic properties of hydrocarbons. *Proteins* **11**, 281–296 (1991).

70. **Acknowledgments:** We thank T. Mayumi for his advice about this research. **Funding:** This study was supported in part by Grants-in-Aid for Scientific Research from the Ministry of Education, Culture, Sports, Science and Technology of Japan and from the Japan Society for the Promotion of Science. This study was also supported in part by Health Labour Sciences Research Grants from the Ministry of Health, Labor and Welfare of Japan; Health Sciences Research Grants for Research on Publicly Essential Drugs and Medical Devices from the Japan Health Sciences Foundation; and The Nagai Foundation Tokyo. **Author contributions:** Y.M., S.T., and Y.T. designed the research; Y.M., T.N., and M.Y. performed the research; Y.M., T.N., and Y. Yamagata analyzed the data; Y. Yoshioka and S.N. contributed new reagents; and Y.M., Y. Yamagata, and Y.T. wrote the paper. **Competing interests:** The authors declare that they have no competing interests. **Accession numbers:** Coordinates and structure factors have been deposited in the PDB with the accession number 3alq.

Submitted 24 February 2010
Accepted 29 October 2010
Final Publication 16 November 2010
10.1126/scisignal.2000954
Citation: Y. Mukai, T. Nakamura, M. Yoshikawa, Y. Yoshioka, S.-i. Tsunoda, S. Nakagawa, Y. Yamagata, Y. Tsutsumi, Solution of the structure of the TNF-TNFR2 complex. *Sci. Signal.* **3**, ra83 (2010).

Yoshida et al. Nanoscale Research Letters 2011, 6:195
http://www.nanoscalereslett.com/content/6/1/195

Nanoscale Research Letters
a SpringerOpen Journal

NANO EXPRESS Open Access

Promotion of allergic immune responses by intranasally-administrated nanosilica particles in mice

Tokuyuki Yoshida[1,2†], Yasuo Yoshioka[1,2,3*†], Maho Fujimura[1,2], Kohei Yamashita[1,2], Kazuma Higashisaka[1,2], Yuki Morishita[1,2], Hiroyuki Kayamuro[1,2], Hiromi Nabeshi[1,2], Kazuya Nagano[2], Yasuhiro Abe[2], Haruhiko Kamada[2,3], Shin-ichi Tsunoda[2,3,4], Norio Itoh[1], Tomoaki Yoshikawa[1,2], Yasuo Tsutsumi[1,2,3*]

Abstract

With the increase in use of nanomaterials, there is growing concern regarding their potential health risks. However, few studies have assessed the role of the different physical characteristics of nanomaterials in allergic responses. Here, we examined whether intranasally administered silica particles of various sizes have the capacity to promote allergic immune responses in mice. We used nanosilica particles with diameters of 30 or 70 nm (nSP30 or nSP70, respectively), and conventional micro-sized silica particles with diameters of 300 or 1000 nm (nSP300 or mSP1000, respectively). Mice were intranasally exposed to ovalbumin (OVA) plus each silica particle, and the levels of OVA-specific antibodies (Abs) in the plasma were determined. Intranasal exposure to OVA plus smaller nanosilica particles tended to induce a higher level of OVA-specific immunoglobulin (Ig) E, IgG and IgG1 Abs than did exposure to OVA plus larger silica particles. Splenocytes from mice exposed to OVA plus nSP30 secreted higher levels of Th2-type cytokines than mice exposed to OVA alone. Taken together, these results indicate that nanosilica particles can induce allergen-specific Th2-type allergic immune responses in vivo. This study provides the foundations for the establishment of safe and effective forms of nanosilica particles.

Introduction

With the recent development of nanotechnology, many nanomaterials with innovative functions have been developed. For example, nanoparticles of titanium dioxide and silica have been used in commercial applications related to medicine, cosmetics and food [1]. In particular, amorphous (noncrystalline) nanosilica particles possess extraordinary advantages, including straightforward synthesis, relatively low cost, and easy surface modification [1,2]. Nanosilica particles are increasingly being used for many applications, including cosmetics, food technology, medical diagnosis, cancer therapy, and drug delivery [1-4].

As the use of nanomaterials increases, there is rising concern regarding their potential health risks because there is preliminary evidence that the unique electrical and mechanical properties of nanomaterials is associated with undesirable biological interactions [5,6]. In addition, it has recently become evident that particle characteristics, including particle size and surface properties, are important factors in pathologic alterations and cellular responses [7-10]. For instance, Nishimori et al have previously demonstrated that nanosilica particles with relatively small particle size induce a greater level of toxicity, including liver injury, than do silica particles with larger particle size [11]. To create safe and effective forms of nanomaterials, studies which provide basic information regarding biological responses to nanomaterials are essential.

Numerous studies have shown that several types of nanomaterials increase the incidence of allergic immune diseases [12-14]. Activation of the Th2 response, including production of interleukin (IL)-4, IL-5, and IL-13 from Th2 cells (a subset of $CD4^+$ T cells) and immunoglobulin (Ig) G1 or IgE from B cells, is responsible for

* Correspondence: yasuo@phs.osaka-u.ac.jp; ytsutsumi@phs.osaka-u.ac.jp
† Contributed equally
[1]Department of Toxicology and Safety Science, Graduate School of Pharmaceutical Sciences, Osaka University, 1-6, Yamadaoka, Suita, Osaka 565-0871, Japan
Full list of author information is available at the end of the article

many of the pathologic features of allergic immune diseases [15]. Some reports have shown that intranasal or airway exposure to nanomaterials promotes allergic immune responses, indicating the immune-activating potential of nanomaterials [12,13]. However, the role of the different physical characteristics of nanomaterials in the production of allergic responses has not been elucidated.

Here, we examined whether intranasal exposure to nanosilica particles has the capacity to promote allergic immune responses in mice. In addition, we investigated the relationship between the size of silica particles and allergic immune responses.

Materials and methods

Silica particles

Amorphous silica particles with a diameter of 30, 70, 300 and 1,000 nm (Micromod Partikeltechnologie, Rostock/Warnemünde, Germany, designated nSP30, nSP70, nSP300 and mSP1000, respectively) were used in this study. The particle numbers of silica particles were 3.5×10^{13}, 2.8×10^{12}, 3.5×10^{10}, or 9.5×10^{8} particles/mg (nSP30, nSP70, nSP300, or mSP1000, respectively). Silica particles were sonicated for 5 min and vortexed for 1 min before use. The size of particles was measured using a Zetasizer Nano-ZS (Malvern Instruments, UK). The mean size and the size distribution of particles were measured by means of dynamic light scattering. We confirmed that the particle size distributions of these silica particles were narrow.

Mice

Female BALB/c mice were purchased from Nippon SLC (Hamamatsu, Japan) and used at 6 to 8 weeks of age. All of the animal experimental procedures in this study were performed in accordance with the National Institute of Biomedical Innovation Guidelines for the Welfare of Animals.

Exposure protocols and detection of antigen-specific antibody responses by enzyme-linked immunosorbent assay

Female BALB/c mice were intranasally exposed to a 20 μL aliquot (10 μL per nostril) containing 10 μg of ovalbumin (OVA; Sigma Chemical Co, St. Louis, MO, USA) as antigen, plus nSP30, nSP70, nSP300, or mSP1000 at concentrations of 10, 50 or 250 μg/mouse, on days 0, 1, and 2. On day 21, plasma was collected to assess antigen-specific antibody (Ab) responses. Antigen-specific IgG and subclass IgG1 Ab levels were determined by enzyme-linked immunosorbent assay (ELISA). The ELISA plates (Maxisorp, type 96F; Nalge Nunc International, Naperville, IL, USA) were coated with 10 μg/ml OVA and incubated overnight at 4°C. Non-specific Ab binding was minimized by incubating the plates with 4% blocking solution (Block Ace; Dainippon Sumitomo Pharmaceuticals, Osaka, Japan) at 37°C for 2 h. Plasma dilutions were added to the antigen-coated plates and incubated at 37°C for a further 2 h. The coated plates were then washed with PBS containing 0.05% Tween 20 and incubated with a horseradish peroxidase-conjugated goat anti-mouse IgG solution (Southern Biotechnology Associates, Birmingham, AL, USA) at 37°C for 2 h. The color reaction was developed with tetramethylbenzidine (MOSS, Inc., Pasadena, MD, USA), stopped with 2N H_2SO_4, and quantitated by measuring OD_{450} minus OD_{655} using a microplate reader. OVA-specific IgE Ab levels in plasma were determined using commercial ELISA kits (Dainippon Sumitomo Pharma, Osaka, Japan).

Isolation of splenocytes

Spleens were aseptically removed and placed in RPMI 1640 medium (Wako Pure Chemical Industries, Osaka, Japan) supplemented with 10% fetal bovine serum, 50 mM 2-mercaptoethanol and 1% antibiotic cocktail (Nacalai Tesque, Kyoto, Japan). The single-cell suspension of splenocytes was treated with ammonium chloride to lyse the red blood cells, and the splenocytes were washed, counted, and suspended in RPMI medium supplemented with 10% fetal bovine serum, 50 mM 2-mercaptoethanol, 1% antibiotic cocktail, 10 mL/L of 100 × nonessential amino acids solution, 1 mM sodium pyruvate, and 10 mM HEPES to a final concentration of 1×10^{7} cells/mL.

Antigen-specific cytokine responses

Antigen-specific cytokine responses were evaluated by culturing the splenocytes (5×10^{6} cells/well) in the presence of OVA (1 mg/mL) in vitro. Cells were incubated at 37°C for 72 h. Culture supernatants from in vitro unstimulated and OVA-stimulated cells were analyzed by the Bio-Plex Multiplex Cytokine Assay (Bio-Rad Laboratories, Hercules, CA, USA) according to the manufacturer's instructions. The assay results were read on a Luminex 100 Multiplex Bio-Assay Analyzer (Luminex, Austin, TX, USA). The difference between the mean concentration of cytokines in supernatants from in vitro OVA-stimulated cells and unstimulated cells (background) was then calculated.

Statistical Analysis

All values are expressed as mean ± SEM. Differences between groups were assessed using analysis of variance followed by Turkey's method.

Results and discussion

Antigen-specific IgE Ab responses to silica particles

To assess the relationship between the size of silica particles and allergic immune responses, we used nanosilica

particles with diameters of 30 or 70 nm (nSP30 or nSP70, respectively), and conventional micro-sized silica particles with diameters of 300 or 1,000 nm (nSP300 or mSP1000, respectively). The mean secondary particle diameters of the silica particles measured by dynamic laser scatter analysis were 33, 79, 326, and 945 nm, respectively (data not shown). We examined the silica particles by transmission electron microscopy, and confirmed that they were well-dispersed smooth-surfaced spheres (data not shown). To investigate the potential of silica particles to enhance allergic immune responses, we examined their effect on the production of allergen-specific Abs responses in vivo. On days 0, 1, and 2, mice were intranasally exposed to OVA (10 μg/mouse) plus silica particles at concentrations of 10, 50, and 250 μg/mouse. On day 21, we collected plasma from the mice and performed an ELISA to examine anti-OVA IgE Ab responses. The levels of IgE Abs tended to be higher in mice exposed to OVA plus smaller nanosilica particles than in mice exposed to OVA plus larger silica particles (Figure 1a). In particular, the OVA-specific IgE Ab level in OVA plus nSP30-exposed mice was significantly higher than in mice exposed to OVA alone (Figure 1a). We consider that this level of IgE Ab would induce the mast cell degranulation and histamine release, which are major mechanisms underlying anaphylactic reactions in allergic diseases [16]. In addition, the OVA-specific IgE Ab response in mice exposed to OVA plus nSP30 increased in an nSP30-dose-dependent manner (Figure 1b). Taken together, these results suggest that nanosilica particles such as nSP30 are capable of inducing allergic immune responses and have the potential to cause serious allergic symptoms.

Antigen-specific IgG Abs subclass responses of silica particles

Next, to assess the types of immune responses elicited by silica particles, we measured the levels of anti-OVA IgG Ab and anti-OVA IgG1 Ab. IgG1 production is indicative of a Th2-type response. The levels of anti-OVA IgG and anti-OVA IgG1 Abs induced by intranasal-exposure to OVA plus smaller silica particles were higher than those induced by OVA plus larger silica particles (Figure 2); this was similar to the results observed for IgE Ab responses, described above (Figure 1). The levels of OVA-specific IgG Ab and OVA-specific IgG1 Ab in mice exposed to OVA plus nSP30 were significantly higher than in those exposed to OVA alone

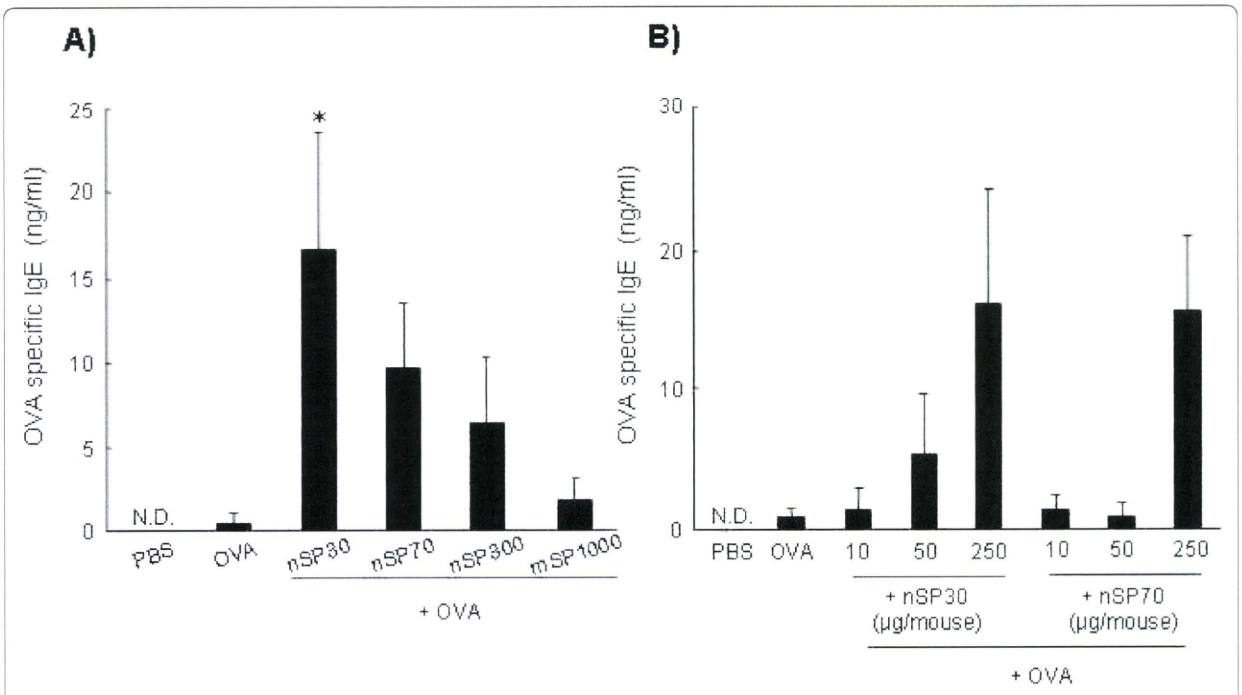

Figure 1 Plasma OVA-specific IgE Ab responses after intranasal exposure to OVA plus silica particles. **(a)** BALB/c mice were intranasally exposed to PBS (vehicle control), OVA alone or OVA plus silica particles (250 μg/mouse) on days 0, 1, and 2. **(b)** BALB/c mice were intranasally exposed to PBS (vehicle control), OVA alone or OVA plus the designated dose of nSP30 or nSP70 on days 0, 1, and 2. Plasma was collected on day 21 and analyzed by ELISA to assess (a) the relationship between silica particle size and OVA-specific IgE Ab responses and (b) the dose-response effect of nSP30 and nSP70 on OVA-specific IgE Ab levels. N.D., not detected. Data are presented as mean ± SEM (n = 8 to 13; *P < 0.05 *vs* OVA alone).

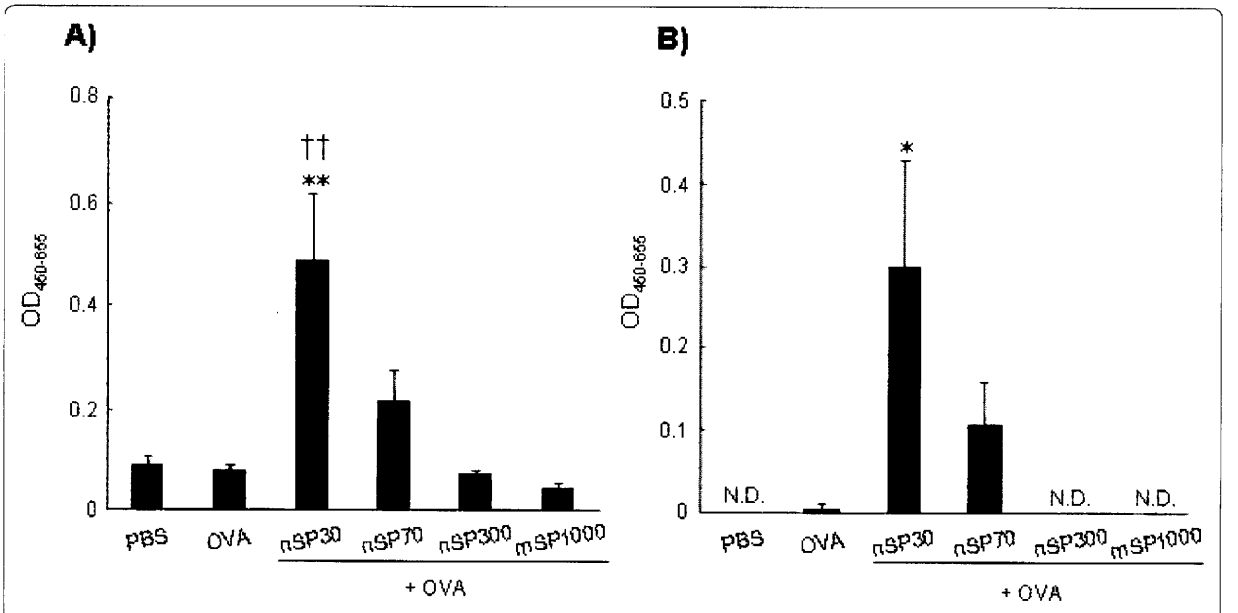

Figure 2 Plasma OVA-specific IgG and subclass IgG1 Ab response after intranasal exposure to OVA plus silica particles. BALB/c mice were intranasally exposed to PBS (vehicle control), OVA alone or OVA plus silica particles (250 μg/mouse) on days 0, 1, and 2. Plasma was collected on day 21 and analyzed by ELISA to detect the level of **(a)** OVA-specific IgG and **(b)** OVA-specific IgG1 Ab responses. Data represent mean absorbance at a wavelength of 450 nm (reference wavelength, 655 nm). N.D., not detected. Data are presented as mean ± SEM (n = 5 to 8); $^{*}P < 0.05$, $^{**}P < 0.01$ vs OVA alone; $^{\dagger\dagger}P < 0.01$ vs PBS).

(Figure 2). These results suggest that nanosilica particles can induce the production of antigen-specific Ab responses including antigen-specific Th2 allergic immune responses.

Antigen-specific cytokine responses of silica particles

To clarify the mechanism by which nSP30 elicited an immune response, we analyzed the profiles of cytokines released from splenocytes of OVA-exposed mice. The splenocytes were cultured in the presence of OVA *in vitro*, and the culture supernatants were assessed for Th2-type cytokines by using a multiplexed immunobeads assay. Splenocytes from mice exposed to OVA plus nSP30 exhibited higher levels of Th2-type cytokines (IL-4 and IL-5) than those induced with OVA alone (Figure 3). In contrast, there was hardly any difference in Th1-type cytokine (IFN-γ) production amongst all of the exposed mice (data not shown). In addition, nSP70, nSP300, and mSP1000 did not induce cytokine production (Figure 3). These results suggest that nSP30 nanosilica particle induces a Th2-type immune response in this experiment.

It is not clear why nanosilica particles such as nSP30 would induce Th2-polarized allergic immunity. Our results support previous reports showing that the immune-activating effect of nanomaterials increases with decreasing particle size [12,17]. The mechanisms behind the immune-activating effect of nanomaterials have not been fully elucidated. Nygaard et al [17] showed that the higher specific surface area of nanomaterials as compared to micro-sized particles allows more antigen to be adsorbed per particle. We consider that one possible mechanism by which allergic immune responses induced by nanosilica particles is that many antigen-captured nanomaterials might be taken up by professional antigen presenting cells, such as dendritic cells. Another possible mechanism is that the nanomaterials induce oxidative stress [18,19]. We have observed that nanosilica particles such as nSP30 are stronger inducers of oxidative stress than larger silica particles (unpublished data). Because there is accumulating evidence that oxidative stress plays a role in pro-inflammatory and immune-activating effects [20,21], dendritic cells might be activated more efficiently by nSP30 than by larger silica particles. Furthermore, we also observed that induction of oxidative stress by nanosilica particles is decreased by surface modification of nanosilica particles (unpublished data). Therefore, surface modification might be one approach to decrease allergic immune responses induced by nanosilica particles.

Conclusion

Here, we show that nanosilica particles have the potential to induce allergic immune responses after intranasal exposure. We consider that further studies of the relationship between the characteristics of nanomaterials

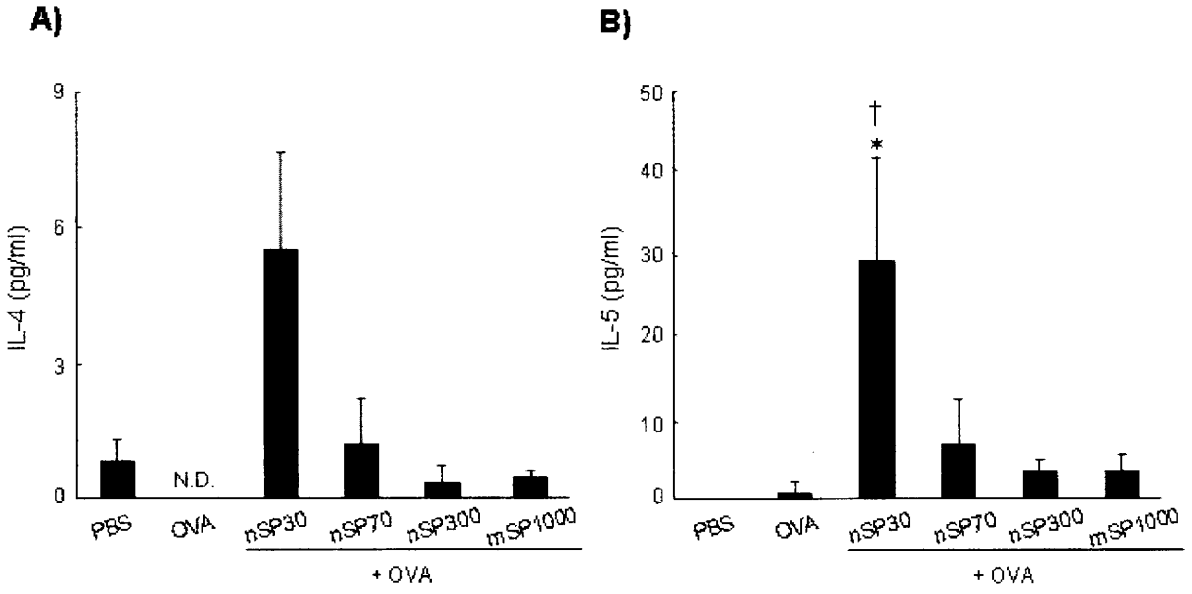

Figure 3 Cytokine responses induced after intranasal exposure to OVA plus silica particles. BALB/c mice were intranasally exposed to PBS (vehicle control), OVA alone or OVA plus silica particles (250 μg/mouse) on days 0, 1, and 2. On day 21, splenocytes from each group were prepared and cultured with 1 mg/mL OVA. Culture supernatants were harvested after 3 days of incubation, and the level of OVA-induced IL-4 (A) and IL-5 (B) produced and released into the culture supernatant was analyzed using the Bio-Plex Multiplex Cytokine Assay. Data are presented as mean ± SEM (n = 3; $^{*}P < 0.05$ vs OVA alone; $^{\dagger}P < 0.05$ vs PBS).

and allergic immune responses will facilitate the development of safe and effective nanomaterials.

Acknowledgements
This study was supported in part by Grants-in-Aid for Scientific Research from the Ministry of Education, Culture, Sports, Science and Technology of Japan, and from the Japan Society for the Promotion of Science. This study was also supported in part by Health Labor Sciences Research Grants from the Ministry of Health, Labor and Welfare of Japan; by Health Sciences Research Grants for Research on Publicly Essential Drugs and Medical Devices from the Japan Health Sciences Foundation; by a Global Environment Research Fund from Minister of the Environment; and by a the Knowledge Cluster Initiative; and by Food Safety Commission; and by The Nagai Foundation Tokyo; and by The Cosmetology Research Foundation; and by The Smoking Research Foundation.

Author details
[1]Department of Toxicology and Safety Science, Graduate School of Pharmaceutical Sciences, Osaka University, 1-6, Yamadaoka, Suita, Osaka 565-0871, Japan [2]Laboratory of Biopharmaceutical Research, National Institute of Biomedical Innovation, 7-6-8 Saito-asagi, Ibaraki, Osaka 567-0085, Japan [3]The Center for Advanced Medical Engineering and Informatics, Osaka University, 1-6, Yamadaoka, Suita, Osaka 565-0871, Japan [4]Department of Biomedical Innovation, Graduate school of Pharmaceutical Sciences, Osaka University, 7-6-8 Saito-asagi, Ibaraki, Osaka 567-0085, Japan

Authors' contributions
TY and YY designed the study; TY, MF, KY, KH, YM and HK performed experiments; TY, YY and MF collected and analysed data; TY and YY wrote the manuscript; HN, KN, YA, HK, ST, NI and TY gave technical support and conceptual advice. YT supervised the all of projects. All authors discussed the results and commented on the manuscript.

Competing interests
The authors declare that they have no competing interests.

Received: 7 October 2010 Accepted: 4 March 2011
Published: 4 March 2011

References

1. Fadeel B, Garcia-Bennett AE: **Better safe than sorry: Understanding the toxicological properties of inorganic nanoparticles manufactured for biomedical applications.** *Adv Drug Deliv Rev* 2010, **62**:362-374.
2. Barik TK, Sahu B, Swain V: **Nanosilica-from medicine to pest control.** *Parasitol Res* 2008, **103**:253-258.
3. Bharali DJ, Klejbor I, Stachowiak EK, Dutta P, Roy I, Kaur N, Bergey EJ, Prasad PN, Stachowiak MK: **Organically modified silica nanoparticles: a nonviral vector for in vivo gene delivery and expression in the brain.** *Proc Natl Acad Sci USA* 2005, **102**:11539-11544.
4. Bottini M, D'Annibale F, Magrini A, Cerignoli F, Arimura Y, Dawson MI, Bergamaschi E, Rosato N, Bergamaschi A, Mustelin T: **Quantum dot-doped silica nanoparticles as probes for targeting of T-lymphocytes.** *Int J Nanomedicine* 2007, **2**:227-233.
5. Kagan VE, Bayir H, Shvedova AA: **Nanomedicine and nanotoxicology: two sides of the same coin.** *Nanomedicine* 2005, **1**:313-316.
6. Nel A, Xia T, Madler L, Li N: **Toxic potential of materials at the nanolevel.** *Science* 2006, **311**:622-627.
7. Albrecht C, Schins RP, Hohr D, Becker A, Shi T, Knaapen AM, Borm PJ: **Inflammatory time course after quartz instillation: role of tumor necrosis factor-alpha and particle surface.** *Am J Respir Cell Mol Biol* 2004, **31**:292-301.
8. He X, Nie H, Wang K, Tan W, Wu X, Zhang P: **In vivo study of biodistribution and urinary excretion of surface-modified silica nanoparticles.** *Anal Chem* 2008, **80**:9597-9603.
9. Morishige T, Yoshioka Y, Inakura H, Tanabe A, Yao X, Narimatsu S, Monobe Y, Imazawa T, Tsunoda S, Tsutsumi Y, Mukai Y, Okada N, Nakagawa S: **The effect of surface modification of amorphous silica particles on NLRP3 inflammasome mediated IL-1beta production, ROS production and endosomal rupture.** *Biomaterials* 2010, **31**:6833-6842.
10. Morishige T, Yoshioka Y, Tanabe A, Yao X, Tsunoda S, Tsutsumi Y, Mukai Y, Okada N, Nakagawa S: **Titanium dioxide induces different levels of IL-1beta production dependent on its particle characteristics through**

caspase-1 activation mediated by reactive oxygen species and cathepsin B. *Biochem Biophys Res Commun* 2010, **392**:160-165.
11. Nishimori H, Kondoh M, Isoda K, Tsunoda S, Tsutsumi Y, Yagi K: **Silica nanoparticles as hepatotoxicants.** *Eur J Pharm Biopharm* 2009, **72**:496-501.
12. de Haar C, Hassing I, Bol M, Bleumink R, Pieters R: **Ultrafine but not fine particulate matter causes airway inflammation and allergic airway sensitization to co-administered antigen in mice.** *Clin Exp Allergy* 2006, **36**:1469-1479.
13. Nygaard UC, Hansen JS, Samuelsen M, Alberg T, Marioara CD, Lovik M: **Single-walled and multi-walled carbon nanotubes promote allergic immune responses in mice.** *Toxicol Sci* 2009, **109**:113-123.
14. Bonner JC: **Nanoparticles as a potential cause of pleural and interstitial lung disease.** *Proc Am Thorac Soc* 2010, **7**:138-141.
15. Finkelman FD, Hogan SP, Hershey GK, Rothenberg ME, Wills-Karp M: **Importance of cytokines in murine allergic airway disease and human asthma.** *J Immunol* 2010, **184**:1663-1674.
16. Yoshida T, Yoshioka Y, Fujimura M, Yamashita K, Higashisaka K, Nakanishi R, Morishita Y, Kayamuro H, Nabeshi H, Nagano K, Abe Y, Kamada H, Tsunoda S, Yoshikawa T, Itoh N, Tsutsumi Y: **Potential adjuvant effect of intranasal urban aerosols in mice through induction of dendritic cell maturation.** *Toxicol Lett* 2010, **199**:383-388.
17. Nygaard UC, Samuelsen M, Aase A, Lovik M: **The capacity of particles to increase allergic sensitization is predicted by particle number and surface area, not by particle mass.** *Toxicol Sci* 2004, **82**:515-524.
18. Brown DM, Wilson MR, MacNee W, Stone V, Donaldson K: **Size-dependent proinflammatory effects of ultrafine polystyrene particles: a role for surface area and oxidative stress in the enhanced activity of ultrafines.** *Toxicol Appl Pharmacol* 2001, **175**:191-199.
19. Shvedova AA, Kagan VE, Fadeel B: **Close encounters of the small kind: adverse effects of man-made materials interfacing with the nano-cosmos of biological systems.** *Annu Rev Pharmacol Toxicol* 2010, **50**:63-88.
20. Swindle EJ, Metcalfe DD: **The role of reactive oxygen species and nitric oxide in mast cell-dependent inflammatory processes.** *Immunol Rev* 2007, **217**:186-205.
21. Martinon F: **Signaling by ROS drives inflammasome activation.** *Eur J Immunol* 2010, **40**:616-619.

doi:10.1186/1556-276X-6-195
Cite this article as: Yoshida *et al.*: Promotion of allergic immune responses by intranasally-administrated nanosilica particles in mice. *Nanoscale Research Letters* 2011 **6**:195.